
VOLUME 143
August 2014
ISSN: 0375-6742
ELSEVIER
JGE
JOURNAL OF
GEOCHEMICAL
EXPLORATION
JOURNAL FOR ENVIRONMENTAL AND ECONOMIC GEOCHEMISTRY
http://www.elsevier.com/locate/jgeoexp

Journal of Geochemical Exploration 143 (2014) 116–126

Contents lists available at ScienceDirect

Journal of Geochemical Exploration

journal homepage: www.elsevier.com/locate/jgeoexp

Two epochs of magmatism and metallogeny in the Cuihongshan Fe-polymetallic deposit, Heilongjiang Province, NE China: Constrains from U–Pb and Re–Os geochronology and Lu–Hf isotopes

Xin-Lu Hu [a], Zhen-Ju Ding [a,*], Mou-Chun He [a,b], Shu-Zhen Yao [a,c], Bo-Peng Zhu [a], Jun Shen [a], Bin Chen [a]

[a] Faculty of Earth Resources, China University of Geosciences, Wuhan 430074, China
[b] State Key Laboratory of Geological Process and Mineral Resources, China University of Geosciences, Wuhan 430074, China
[c] Key Laboratory of Tectonics and Petroleum Resources, Ministry of Education, Wuhan 430074, China

ARTICLE INFO

Article history:
Received 31 August 2013
Accepted 26 March 2014
Available online 8 April 2014

Keywords:
U–Pb geochronology
Lu–Hf isotope
Molybdenite Re–Os age
Cuihongshan
Heilongjiang Province
NE China

ABSTRACT

The large-sized Cuihongshan Fe-polymetallic deposit is located in the north segment of the Lesser Xing'an range, NE China. The Fe orebodies are dominantly hosted in the contact zone between the alkali–feldspar granite and the dolomitic crystalline limestones or skarns, whereas the Pb–Zn (Cu) and W–Mo orebodies are mostly hosted in the contact zone between the syenogranite and skarns, as well as within the syenogranite. The alkali–feldspar granite and syenogranite yield zircon U–Pb ages of 491.1 ± 2.4 Ma and 199.8 ± 1.8 Ma, with $\varepsilon_{Hf}(t)$ values of −3.7 to −1.3 and 2.5 to 3.9, respectively. Both of them are characterized by high SiO_2 and $Na_2O + K_2O$ content, enrichment in Rb, Th, U and Pb, and depletion in Ba, Sr, Nb, Ta, P, Ti and Eu, indicating an A-type affinity. The Re–Os model ages of the molybdenite range from 198.0 to 202.1 Ma. These data suggest that the Fe-related alkali–feldspar granite was formed by partial melting of the Mesoproterozoic crust in an extensional setting after the final collision between the Xing'an and Songnen Blocks, while the Pb–Zn (Cu) and W–Mo-related syenogranite was probably generated by crystal fractionation from depleted-mantle-derived magmas, which are products of lithospheric delamination.

1. Introduction

Cuihongshan is one of the largest Fe-polymetallic deposit discovered in Heilongjiang Province, NE China. The deposit yields proven resources of 68.35 Mt Fe, 0.09 Mt Mo, 0.12 Mt W, and 0.51 Mt Zn with average grades of 48% Fe, 0.134% Mo, 0.153% W and 3% Zn.

Several recent studies have been carried out on the deposit geology, fluid inclusion characteristics, S isotope composition of the sulfides as well as the U–Pb age of the syenogranite (previously named as monzogranite) (Du et al., 2011; He et al., 2010; Li et al., 2011). It was recognized as a skarn type deposit and the Fe, Pb–Zn (Cu), W and Mo mineralization were considered to be generated in different metallogenetic stages (He et al., 2010; Li et al., 2011; Shao et al., 2011). However, according to the occurrences of the orebodies and the ore characters, a two-epoch metallogenetic model is preferred for the formation of the Cuihongshan deposit: the early-epoch Fe mineralization associated with the alkali–feldspar granite and the late-epoch Pb–Zn (Cu) and W–Mo mineralization related to the syenogranite. In this paper, we present detailed geochemistry, U–Pb geochronology and Lu–Hf isotope data on the ore-forming-related alkali–feldspar granite and syenogranite, together with Re–Os isotopic dating of the molybdenite, in order to characterize the ore-forming stage, and to constrain the tectonic setting for magmatism and mineralization in the Cuihongshan area.

2. Regional geological setting

The Cuihongshan Fe-polymetallic deposit is located in the north segment of the Lesser Xing'an range, east of the Central Asian Orogenic Belt (CAOB). The Lesser Xing'an range is part of the Songnen Block, which straddles the Xing'an Block in the northwest and the Jiamusi Block in the east, separated by the Hegenshan–Heihe Fault and the Jiayin–Mudanjiang Fault respectively (Fig. 1a) (Wu et al., 2000; Yang et al., 2012; Zhou et al., 2010). Regional geological research has suggested that the Lesser Xing'an range is a complex tectonic region that experienced the closure of the Paleo-Asian Ocean in the Paleozoic, the closure of the Mongol–Okhotsk Ocean in the Late Paleozoic–Mesozoic, and the subduction of the Pacific Plate in the Mesozoic–Cenozoic (Li, 2006; Wang and Mo, 1995; Wu et al., 2000; Xu et al., 1994). The complicated geological evolution history has resulted in intense magmatism as well as extensive mineralization of

* Corresponding author at: 388, Lumo Road, Hongshan District, China University of Geosciences, Wuhan 430074, China. Tel./fax: +86 02767883051.
E-mail address: dingzhenju@163.com (Z.-J. Ding).

http://dx.doi.org/10.1016/j.gexplo.2014.03.027
0375-6742/

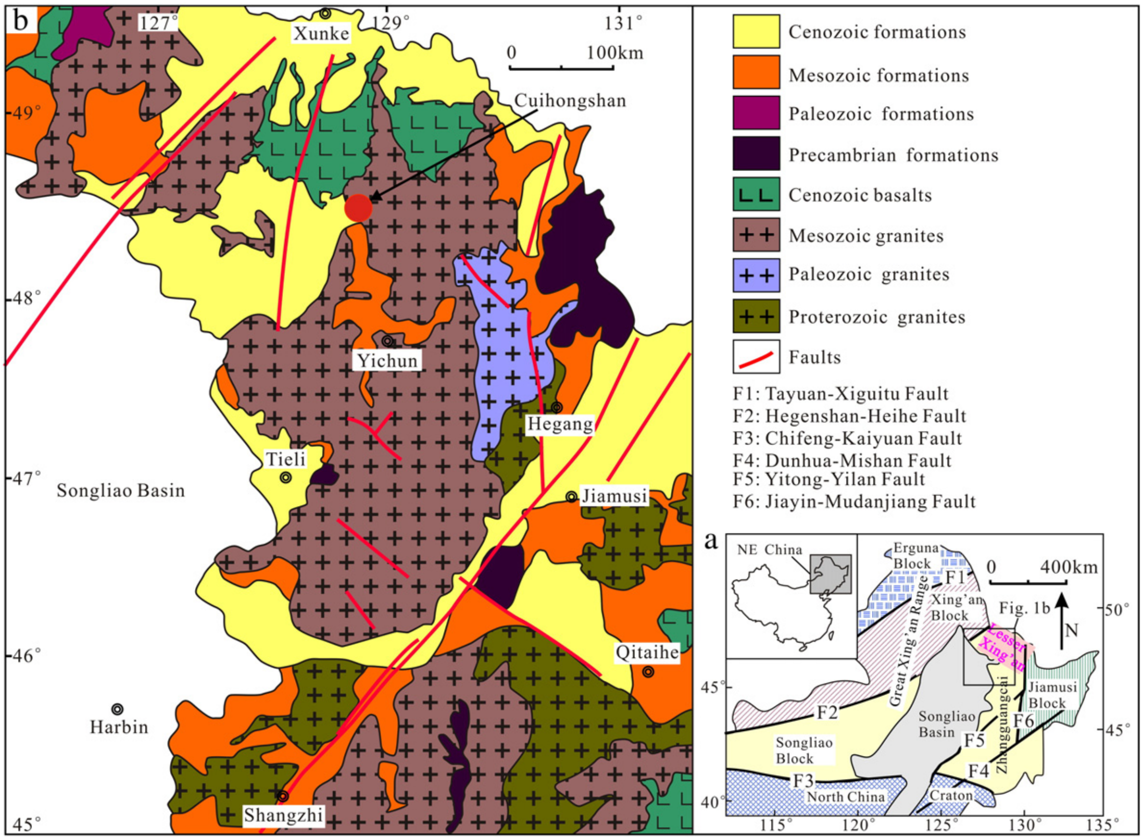

Fig. 1. (a) Tectonic framework of NE China (modified from Wu et al., 2000, 2007). (b) Simplified geological map of the Lesser Xing'an range (modified from Zhang et al., 2010a).

precious metals and nonferrous metals in this area (Ge et al., 2007; Han et al., 1995; Mao et al., 2003).

The stratigraphic sequence outcropping in this area can be generally divided into four units: 1) the Precambrian crystalline basement composed predominantly of the Paleoproterozoic Dongfengshan Group and Zhangguangcailing Group; 2) the Paleozoic submarine sedimentary cover including Cambrian, Ordovician and Permian strata; 3) the Mesozoic continental volcanic sedimentary rocks; 4) the Cenozoic sandstones, conglomerates and alkaline basalts (Fig. 1b). The Precambrian and Paleozoic formation are scattered across the Lesser Xing'an range. The Precambrian metamorphic rocks are dominated by marbles, phyllites, schists, amphibolites, gneisses and granulites (Han et al., 1995; Yang et al., 2012), unconformably overlain by the Paleozoic marine formation. The Cambrian strata, which host numerous skarn type Pb, Zn, W and Mo deposits (Zhao et al., 2009), consist of carbonates and terrigenous clastic rocks. The Ordovician strata can be divided into two lithological sequences: the lower sequence consisting of intermediate-acidic volcanics and the upper sequence consisting of slates, sandstones and conglomerates (Han et al., 1995). In comparison, the Permian strata are mainly made up of sandstones, conglomerates and intercalated limestones (Yang et al., 2012; Yin and Ran, 1997; Zhang et al., 2010b). The Mesozoic terrestrial formation contains terrigenous clastic and volcanic rocks which are extensively distributed throughout the Lesser Xing'an range (Sun et al., 2013; Wu et al., 2007).

Apart from the volcanic rocks, the Lesser Xing'an range is also characterized by widespread plutonic rocks formed at various times: 1) Late Proterozoic granodiorites and alkali–feldspar granites with Rb–Sr and Sm–Nd ages of 614–672 Ma (Yin and Ran, 1997); 2) Early Paleozoic granodiorites, tonalites, monzogranites and alkali–feldspar granites (Han et al., 1995); 3) Late Paleozoic alkali–feldspar granites and alkaline granites (Sun et al., 2001); 4) Early Mesozoic moyites and alkali–feldspar granites; 5) Late Mesozoic quartz diorites, granodiorites and granite porphyries. The Late Proterozoic and Late Paleozoic granites only outcrop sporadically in this region. While the relatively extensive Early Paleozoic granites distribute as an overall SN trending belt in the east of the Lesser Xing'an range. The Mesozoic granites, however, cover the maximum area of the Lesser Xing'an range. According to previous studies, the Mesozoic volcanic and plutonic rocks are considered as products of lithospheric delamination in response to the subduction of the Paleo-Pacific Plate (Ge et al., 2007; Wu et al., 2005, 2007), or alternatively related to the extension after the final closure of the Paleo-Asian Ocean (Mao et al., 2003, 2005; Qi et al., 2005).

3. Geology of the Cuihongshan deposit

The only exposed stratum in the Cuihongshan area is the Lower Cambrian Qianshan Formation, which consists predominantly of dolomitic crystalline limestones, sandstones, siltstones and slates (Fig. 2a and b). The stratum was intruded by the alkali–feldspar granite and the syenogranite. The alkali–feldspar granite (Fig. 3a) is distributed in the north section and south section of the mining district. It was intruded by the syenogranite (previously named as monzogranite, Fig. 3b, Li et al., 2011; Shao et al., 2011), which mainly outcrops in the west section and the east section. Both the alkali–feldspar granite and the syenogranite occur as stocks and they are locally separated by the NNE and near WE trending faults.

The mineralizations in Cuihongshan and adjacent areas are constrained by a series of NE trending composite folds, which are cut-off by NW trending faults (Shao et al., 2011). The orebodies in the Cuihongshan deposit are predominantly controlled by three types of structures: the intrusive contact zone between the plutonic rocks and wall rocks; the interformational fracture zones within the

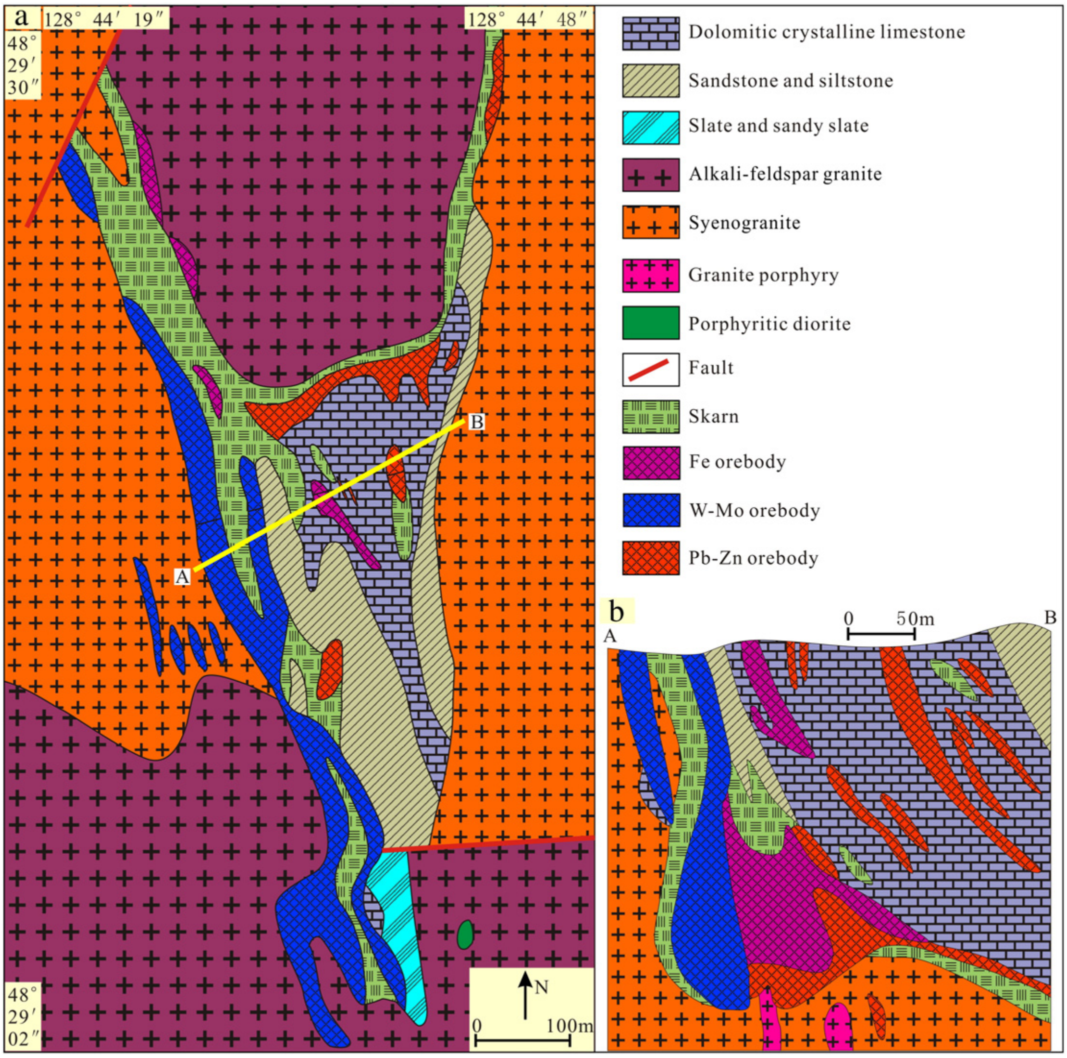

Fig. 2. (a) Sketch geological map of the Cuihongshan mining district (modified from Li et al., 2011; Shao et al., 2011). (b) Cross-section showing the geology along the 54 exploration line.

Qianshan Formation; the intersection of the NNE and NWW trending faults. Up to now, a total of 106 cystiform, lenticular or veined orebodies have been discovered. Most of the Fe orebodies are hosted in the contact zone between the alkali–feldspar granite and the dolomitic crystalline limestones or skarns (Figs. 2a, 3c and d), showing a genetic link between the Fe mineralization and the alkali–feldspar granite. The largest orebody, No. I orebody, extends 400 m in length, 200 m in maximum thickness and has been mined about 8.31 Mt Fe. Whereas the Pb–Zn (Cu) and W–Mo orebodies, together with a lesser amount of low-grade Fe orebodies, are hosted in the contact zone between the syenogranite and the skarns, as well as within the syenogranite (Figs. 2b, 3e and f), indicating an association between the Pb–Zn–(Cu)–W–Mo mineralization and the syenogranite.

The ore mineralogy contains magnetite, molybdenite, scheelite, sphalerite, galena, pyrite and chalcopyrite, with minor cassiterite, arsenopyrite, and pyrrhotite (Fig. 3g–i). The magnetite, sphalerite, galena, and chalcopyrite ores hosted in the skarns are dominated by massive, veined and disseminated structures, whereas the scheelite and molybdenite ores developing within the syenogranite are commonly characterized by veinlet-disseminated structures. According to the occurrences of the orebodies and the paragenetic association of minerals, two distinct metallogenic systems have been recognized in the Cuihongshan deposit: (1) the alkali–feldspar–granite-related Fe metallogenic system; (2) the syenogranite-related Pb–Zn–(Cu)–W–Mo metallogenic system. The first ore system produced most of the Fe orebodies, and can be subdivided into three stages. Stage I is relatively weakly developed and is characterized by diopside and garnet alteration. Stage II is intensively developed and produces alteration minerals of tremolite, actinolite and epidote, together with immense volumes of magnetite mineralization. Stage III is weakly developed and forms minor phlogopite, epidote and pyrrhotite. The second ore system produces the majority of the Pb–Zn (Cu) and W–Mo orebodies, and involves four stages of alteration and mineralization. Stage I is represented by diopside, garnet and idiocrase alteration, and scheelite mineralization. Stage II is characterized by alteration minerals of actinolite, tremolite, epidote and chlorite, accompanied by magnetite mineralization in the periphery of the scheelite orebodies. Although magnetite mineralization occurred in this stage, they generally form low-grade Fe orebodies and are negligible compared to the Fe orebodies formed in the first ore system. Stage III produces alteration minerals of epidote, chlorite and accessory quartz, together with molybdenite mineralization overprinting the early-stage scheelite orebodies. Stage IV generates quartz, hydromica and kaolinite alteration, associated with mineralization of sphalerite, galena and chalcopyrite.

In summary, the Fe mineralization is mostly associated with the alkali–feldspar granite, while the Pb–Zn (Cu) and W–Mo mineralization is genetically related to the syenogranite. The early-epoch Fe

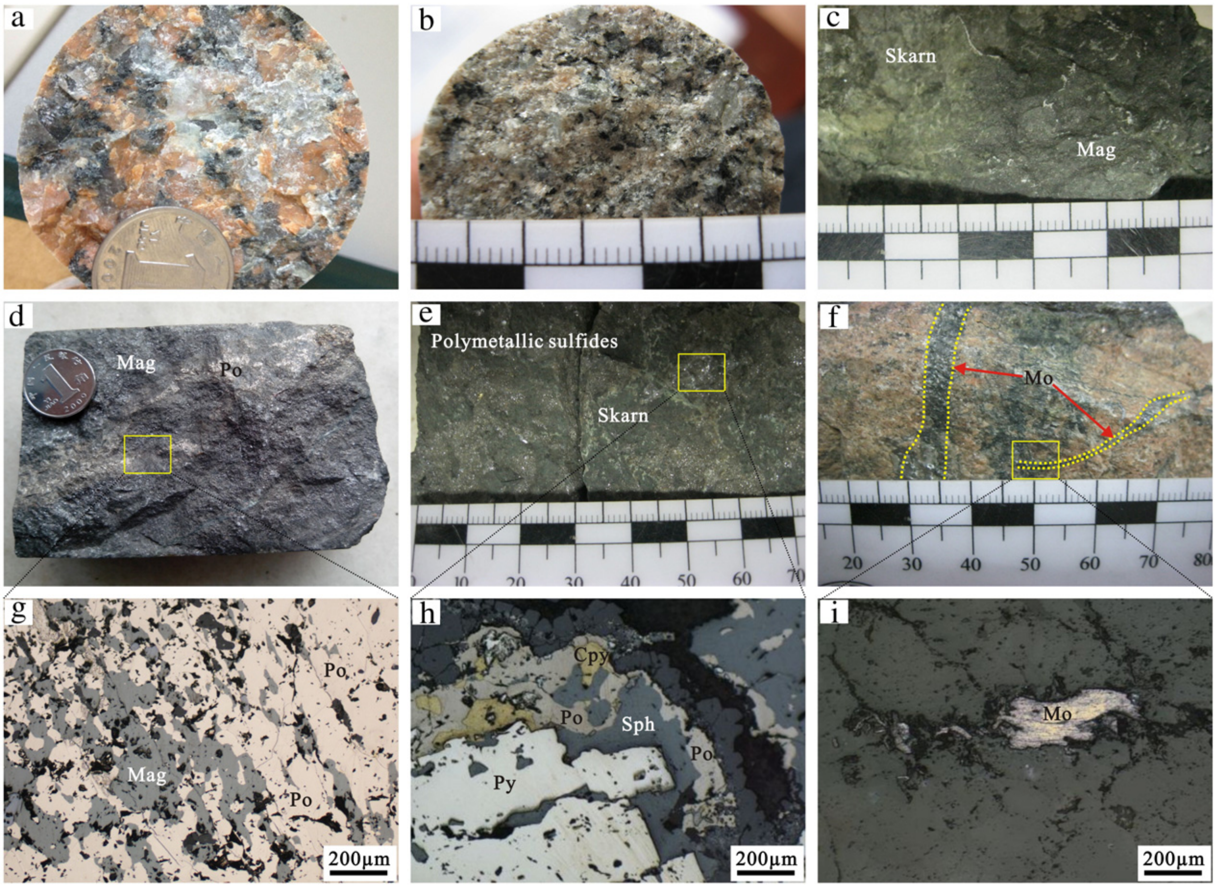

Fig. 3. Characteristics of the plutons and ores in the Cuihongshan deposit. (a) alkali–feldspar granite; (b) syenogranite; (c) skarns with magnetite mineralization in the contact zone between the alkali–feldspar granite and the dolomitic crystalline limestones; (d) massive magnetite ore; (e) polymetallic sulfides hosted in the skarns outside the syenogranite; (f) veinlet and disseminated molybdenite within the syenogranite; (g) microscopic picture showing the coexisting magnetite and pyrrhotite; (h) microscopic picture showing mineral assemblage consisting of pyrite, chalcopyrite, sphalerite and pyrrhotite; (i) microscopic picture showing the disseminated molybdenite. Abbreviations in figure: Mag — magnetite; Po — pyrrhotite; Mo — molybdenite; Gn — galena; Sph — sphalerite; Py — pyrite; Cpy — chalcopyrite.

mineralization is locally overlain or modified by the late-epoch Pb–Zn (Cu) and W–Mo mineralization.

4. Petrography and analytical methods

4.1. Petrography

The alkali–feldspar granite contains dominant minerals of K-feldspar (~55 vol.%, 2–6 mm), quartz (~30 vol.%, 2–4 mm), plagioclase (~5 vol.%, 2–4 mm), biotite (~5 vol.%, 0.1–2 mm) and chlorite (~3 vol.%, 0.2–2 mm), with minor apatite, titanite, sericite and zircon. The K-feldspars occur mostly as subhedral microcline with subordinate orthoclase and anorthoclase. The quartz grains are irregular. The small quantity of plagioclases are subhedral–anhedral with polysynthetic twinning.

The syenogranite is dominated by minerals of K-feldspar (~45 vol.%, 0.1–1.5 mm), quartz (~30 vol.%, 0.1–2.5 mm), plagioclase (~15 vol.%, 0.1–2 mm) and biotite (~5 vol.%, 0.1–0.5 mm), with chlorite, epidote, biotite, apatite and zircon as accessory minerals. The K-feldspars are platy and dominated by euhedral–subhedral orthoclase, microcline and perthite. The quartz grains are generally irregular. The plagioclases are subhedral–anhedral and few of them have been locally altered to sericites. Sporadic chloritization and epidotization are also observed. Previous studies have considered this pluton as monzogranite (Li et al., 2011; Shao et al., 2011), but in this study, based on detailed microscopic observation, the content of the K-feldspars is triple that of the plagioclases, indicating that this pluton is mostly syenogranite.

4.2. Analytical methods

4.2.1. Major and trace element analyses

Based on petrographic examination, a total of six samples from different drill holes were selected for geochemical analysis. The samples were crushed in a steel jaw crusher and then powdered to 200-mesh in an agate ball mill. Major element compositions were determined by X-ray fluorescence spectroscope (XRF) (Magix_pro2440) techniques at Hubei Geological Research Laboratory. The analytical uncertainties are generally within 5%. Trace elements determinations were performed using ICP-MS (Agilent 7500a) with a lithium borate fusion at State Key Laboratory of Geological Process and Mineral Resources, China University of Geosciences, Wuhan. Details of the procedures follow Liu et al. (2008a). The analytical accuracy is greater than 10% for most elements.

4.2.2. Zircon U–Pb dating

Zircons from two samples (CHS-011 from the alkali–feldspar granite and CHS-021 from the syenogranite) were separated by means of conventional heavy liquid and magnetic techniques. Cathodoluminescence (CL) images were carried out using a Gatan MonoCL3+ cathode fluorescence spectroscopy at State Key Laboratory of Continental Dynamics, Northwest University, in order to examine the internal textures of zircons and select the appropriate sites for U–Pb analyses. The U–Pb analyses were performed by laser ablation ICP-MS techniques at the State Key Laboratory of Geological Processes and Mineral Resources, China University of Geosciences, Wuhan. A GeoLas

2005 laser ablation system and an Agilent 7500a ICP-MS were combined for the experiments. Details of the operating conditions and parameters are the same as Liu et al. (2008b, 2010). The laser operating conditions were 8-Hz repetition rate, 70-mJ laser energy with spot sizes of 32 μm. Zircon 91500, used as external standard to calibrate the accuracy of analyses, was analyzed twice after every 5 analyses. Analytical data was processed using ICPMSDataCal (Liu et al., 2008b, 2010) and the concordia diagrams were made using Isoplot (ver 3.0) (Ludwig, 2003).

4.2.3. Zircon Lu–Hf isotope analyses

In situ zircon Lu–Hf isotope analyses were subsequently carried out at the State Key Laboratory of Geological Processes and Mineral Resources, China University of Geosciences, Wuhan. Lu–Hf isotopic compositions were determined using a Neptune Plus MC–ICP-MS combined with a Geolas 2005 excimer ArF laser ablation system. Detailed descriptions for operating conditions follow Hu et al. (2012). A laser ablation size of 44 μm and a laser repetition of 10 Hz were used for analyses. Interference of ^{176}Yb on ^{176}Hf was corrected by measuring ^{173}Yb isotope and using $^{176}Yb/^{173}Yb = 0.79381$ (Segal et al., 2003) to calculate $^{176}Yb/^{177}Hf$. Analogously, the interference of ^{176}Lu on ^{176}Hf was corrected by measuring the intensity of ^{175}Lu isotope and using $^{176}Lu/^{175}Lu = 0.02656$ (Blichert-Toft et al., 1997) to calculate $^{176}Lu/^{177}Hf$.

4.2.4. Re–Os isotope analyses

One sample with veinlet molybdenite mineralization (CHS-10), one with disseminated molybdenite mineralization (CHS-12), and one containing quartz–molybdenite veinlets (CHS-13) were selected for Re–Os isotopic analyses. Molybdenites were separated by conventional heavy liquid techniques and further purified by handpicking under a binocular microscope. The Re–Os isotope determinations were performed in the Re–Os Laboratory, National Research Center of Geoanalysis, Chinese Academy of Geological Sciences, Beijing. A Thermo Electron TJA X-series ICP-MS was used for analyses. Detailed analytical procedures have been described by Du et al. (1995, 2004), Mao et al. (1999), Selby and Creaser (2004), and Stein et al. (2003). The model ages were calculated following the equation: $t = [\ln(1 + {}^{187}Os/{}^{187}Re)]/\lambda$, where $\lambda = 1.666 \times 10^{-11}$/year, representing the decay constant of ^{187}Re (Smoliar et al., 1996).

5. Results

5.1. Major and trace elements

Although alteration is observed in both the alkali–feldspar granite and the syenogranite, the total amount of alteration minerals is still negligible (<5 vol.%), and the LOI values of the analyzed samples are all below 1.2 wt.% (Table 1), suggesting that the geochemical data are credible.

Major and trace element compositions of the alkali–feldspar granite and the syenogranite samples are presented in Table 1. The SiO_2 contents of the alkali–feldspar granite range from 71.26 to 71.41 wt.%, with $Na_2O + K_2O$ concentrations of 8.66 to 8.67 wt.%. The samples are potassium-rich, with K_2O/Na_2O ratios between 1.49 and 1.59, classifying them into shoshonitic series (Fig. 4a). In the A/NK–A/CNK diagram (Fig. 4b), the alkali–feldspar granite samples plot on the boundary between the metaluminous field and the paraluminous field with A/CNK (molar $Al_2O_3/(CaO + Na_2O + K_2O)$) values of 1.00 to 1.01. The syenogranite is also characterized by high SiO_2 contents ranging from 69.71 to 70.70. The analyzed four samples have total alkalis ($K_2O + Na_2O$) of 8.51 to 8.90 wt.% and a K_2O/Na_2O ratio of 1.01 to 1.04, plotting in the high-K calc-alkaline field in the K_2O versus SiO_2 diagram (Fig. 4a). The syenogranite has A/CNK values of 0.97 to 1.00, indicating its metaluminous character (Fig. 4b).

Table 1
Major oxides (wt.%) and trace elements (ppm) of the alkali–feldspar granite and syenogranite from the Cuihongshan deposit.

Rock type	Alkali–feldspar granite		Syenogranite			
Sample no.	CHS-011	CHS-013	CHS-021	CHS-023	CHS-031	CHS-033
Na_2O	3.35	3.48	4.39	4.42	4.18	4.20
MgO	0.37	0.36	0.56	0.56	0.58	0.56
Al_2O_3	14.03	13.91	14.65	14.64	14.60	14.63
SiO_2	71.26	71.41	70.70	70.59	69.71	69.87
P_2O_5	0.07	0.07	0.08	0.09	0.10	0.09
K_2O	5.31	5.19	4.44	4.48	4.35	4.31
CaO	1.43	1.38	1.63	1.62	1.69	1.70
TiO_2	0.32	0.31	0.34	0.33	0.38	0.38
MnO	0.04	0.04	0.08	0.08	0.07	0.07
Fe_2O_3	0.47	0.46	0.60	0.51	0.56	0.59
FeO	2.18	2.12	1.88	1.95	2.05	2.02
H_2O^+	0.87	0.88	0.43	0.50	0.95	0.90
CO_2	0.11	0.21	0.04	0.04	0.60	0.50
LOI	0.83	0.87	0.28	0.31	1.15	1.18
Total	100.64	100.69	100.10	100.12	100.97	101.00
$Na_2O + K_2O$	8.66	8.67	8.83	8.90	8.53	8.51
K_2O/Na_2O	1.59	1.49	1.01	1.01	1.04	1.03
A/NK	1.24	1.22	1.22	1.21	1.26	1.26
A/CNK	1.01	1.00	0.98	0.97	0.99	1.00
Li	25.3	25.6	28.5	3.75	15.4	15.5
Be	6.70	6.69	3.54	14.4	3.51	3.79
Sc	5.74	5.85	4.26	2.02	4.70	4.71
V	9.08	9.19	14.8	2.50	16.3	17.0
Cr	1.94	2.39	2.38	1.79	2.02	1.75
Co	24.2	24.3	21.2	40.1	43.8	41.5
Ni	0.71	0.78	1.08	1.74	1.52	1.27
Cu	4.93	3.34	3.92	15.3	2.87	3.86
Zn	43.0	41.5	72.5	704	52.2	54.7
Ga	23.6	24.1	18.9	18.5	18.9	19.2
Rb	344	325	170	587	166	171
Sr	175	169	167	169	187	181
Y	52.3	53.4	35.9	102	35.9	36.0
Zr	274	268	285	128	275	285
Nb	16.8	17.0	13.7	50.0	13.1	13.7
Mo	1.94	1.91	2.25	955	3.52	4.04
Sn	20.3	18.6	2.40	91.0	2.48	2.71
Cs	8.97	8.85	4.07	3.88	2.88	2.91
Ba	451	449	697	506	664	668
La	75.5	80.2	45.1	73.6	47.9	50.1
Ce	155	165	88.4	152	93.3	97.0
Pr	17.1	17.9	9.60	15.7	10.1	10.6
Nd	61.0	65.5	34.0	48.6	36.1	37.2
Sm	11.9	12.5	6.22	9.69	6.67	6.71
Eu	0.90	0.89	1.02	0.17	1.06	1.05
Gd	9.88	10.2	5.22	8.16	5.46	5.54
Tb	1.55	1.58	0.87	1.62	0.91	0.90
Dy	9.04	9.11	5.50	11.4	5.58	5.48
Ho	1.70	1.75	1.14	2.45	1.17	1.14
Er	4.78	4.76	3.45	8.50	3.46	3.49
Tm	0.73	0.73	0.52	1.57	0.56	0.54
Yb	4.48	4.59	3.71	11.9	3.75	3.69
Lu	0.67	0.69	0.61	1.91	0.61	0.59
Hf	8.27	7.97	7.44	6.12	7.19	7.45
Ta	1.42	1.47	1.17	5.45	1.21	1.18
Tl	3.68	3.64	1.16	5.88	1.16	1.18
Pb	30.6	30.6	28.1	130	22.3	22.9
Th	39.4	43.1	18.7	69.2	20.0	19.8
U	12.0	11.0	5.95	41.0	6.34	6.57
LREE	322	342	184	299	195	203
HREE	85	87	57	150	57	57
$\sum$REE	407	429	241	449	252	260
$(La/Yb)_N$	11.4	11.8	8.2	4.2	8.6	9.2

Both the alkali–feldspar granite and the syenogranite display LREE enrichment with $(La/Yb)_N$ ratios of 11.4 to 11.8 and 4.2 to 9.2 respectively. The alkali–feldspar granite has a higher total REE content (ΣREE) (407–429 ppm) compared to the syenogranite (241–449 ppm). The alkali–feldspar granite show strong negative Eu anomalies with Eu/Eu* values of 0.23 to 0.25, whereas three samples from the syenogranite yield Eu/Eu* values of 0.51 to 0.53, the

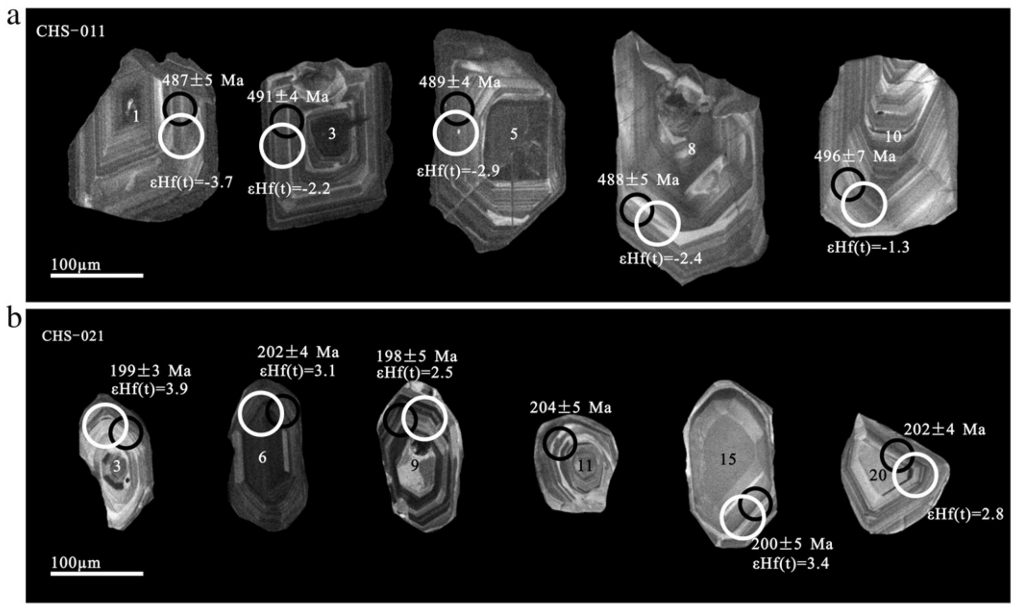

Fig. 4. K_2O vs. SiO_2 diagram (a) and A/NK [molar ratio $Al_2O_3/(Na_2O + K_2O)$] vs. A/CNK [molar ratio $Al_2O_3/(CaO + Na_2O + K_2O)$] diagram (b) of the alkali–feldspar granite and the syenogranite. (a) is from Rickwood (1989).

other one sample possesses Eu/Eu* value of 0.06 (Fig. 5a). Sample CHS-023 shows different REE pattern with the other three samples of syenogranite, possibly suggesting that it was altered. Both the alkali–feldspar granite and the syenogranite are enriched in Rb, Th, U and Pb and depleted in Ba, Sr, Nb, Ta, P and Ti (Fig. 5b), which is typical of A-type granites.

5.2. Zircon U–Pb geochronology

Zircons in the alkali–feldspar granite are colorless and transparent, mostly euhedral–subhedral, ranging from 80 to 200 μm in size, with length/width ratios of 1 to 2/1. The zircon grains have relatively low Th/U ratios of 0.22 to 0.42 (Table 2), possibly due to the high U content of the parental magma. All the zircons display apparent oscillatory zoning in the CL images (Fig. 6), indicating their magmatic origin. 17 analyses yield a concordant group with a weighted mean $^{206}Pb/^{238}U$ age of 491.1 ± 2.4 Ma (Fig. 7), which represents the crystallization age of the alkali–feldspar granite.

Zircons in the syenogranite are also euhedral–subhedral, colorless and transparent. The zircon grains range from 50 to 130 μm in size, with length/width ratios of 1 to 2.5/1. All of them show apparent oscillatory zoning in the CL images (Fig. 6) and have high Th/U ratios (0.36–1.22) (Table 2), indicating their magmatic origin. 14 analyses form a concordant cluster with a weighted mean $^{206}Pb/^{238}U$ age of 199.8 ± 1.8 Ma (Fig. 7), consistent with previous studies (192–199 Ma; Li et al., 2011; Shao et al., 2011). This age is considered as the crystallization age of the syenogranite.

5.3. Lu–Hf isotopes

The same zircons selected for U–Pb dating were subsequently used for in situ Hf isotopic analyses. The results are listed in Table 3 and plotted in Fig. 8. The alkali–feldspar granite yield $^{176}Hf/^{177}Hf$ ratios of 0.282370 to 0.282434 and $\varepsilon_{Hf}(t)$ values of −3.7 to −1.3, with crustal model ages (T_{DM2}) ranging from 1414 to 1539 Ma. While the syenogranite show $^{176}Hf/^{177}Hf$ ratios of 0.282726 to 0.282765 and

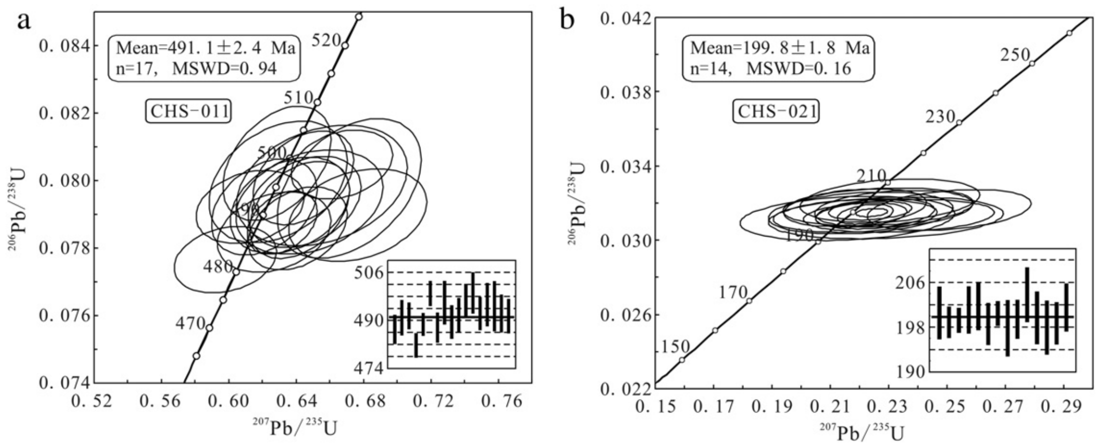

Fig. 5. Chondrite-normalized REE patterns (a) and Primitive Mantle (PM) normalized trace element diagrams (b) of the alkali–feldspar granite and the syenogranite. The chondrite and PM values are from Sun and McDonough (1989).

Table 2
LA–ICP-MS U–Pb data of zircons from the alkali–feldspar granite and syenogranite.

Spot no.	Th (ppm)	U (ppm)	Th/U	Isotopic ratios						Ages (Ma)			
				$^{207}Pb/^{206}Pb$	1σ	$^{207}Pb/^{235}U$	1σ	$^{206}Pb/^{238}U$	1σ	$^{207}Pb/^{235}U$	1σ	$^{206}Pb/^{238}U$	1σ
CHS-011 (alkali–feldspar granite)													
1	208	578	0.36	0.05786	0.00213	0.62714	0.02228	0.07847	0.00078	494	14	487	5
2	146	655	0.22	0.05824	0.00165	0.64240	0.01962	0.07913	0.00095	504	12	491	6
3	125	529	0.24	0.05568	0.00194	0.61251	0.02119	0.07922	0.00072	485	13	491	4
4	148	533	0.28	0.05528	0.00187	0.59611	0.02006	0.07758	0.00065	475	13	482	4
5	336	891	0.38	0.05756	0.00120	0.63168	0.01374	0.07875	0.00061	497	9	489	4
6	239	630	0.38	0.05948	0.00166	0.64004	0.01829	0.07714	0.00061	502	11	479	4
7	246	839	0.29	0.05963	0.00175	0.66721	0.01988	0.08047	0.00067	519	12	499	4
8	160	526	0.30	0.05877	0.00175	0.64101	0.01941	0.07857	0.00081	503	12	488	5
9	124	548	0.23	0.06758	0.00247	0.73884	0.02740	0.07871	0.00082	562	16	488	5
10	183	589	0.31	0.05670	0.00234	0.62931	0.02715	0.07996	0.00118	496	17	496	7
11	220	709	0.31	0.06214	0.00244	0.67787	0.02701	0.07888	0.00091	525	16	489	5
12	159	497	0.32	0.05808	0.00213	0.63644	0.02341	0.07926	0.00093	500	15	492	6
13	378	954	0.40	0.05827	0.00183	0.64428	0.01962	0.08006	0.00092	505	12	497	5
14	497	1468	0.34	0.05619	0.00181	0.62851	0.02134	0.08050	0.00113	495	13	499	7
15	492	1201	0.41	0.05855	0.00199	0.64511	0.02215	0.07935	0.00089	505	14	492	5
16	74	262	0.28	0.05949	0.00305	0.65553	0.03355	0.07985	0.00118	512	21	495	7
17	103	371	0.28	0.06108	0.00254	0.67182	0.02816	0.07976	0.00137	522	17	495	8
18	90	314	0.28	0.05921	0.00265	0.64798	0.02895	0.07936	0.00102	507	18	492	6
19	286	683	0.42	0.05654	0.00184	0.62119	0.02067	0.07921	0.00094	491	13	491	6
20	146	459	0.32	0.05901	0.00207	0.66927	0.02355	0.08209	0.00113	520	14	509	7
CHS-021 (syenogranite)													
1	101	148	0.68	0.05809	0.00443	0.25109	0.01846	0.03160	0.00074	227	15	201	5
2	73	158	0.46	0.06737	0.00457	0.25502	0.01585	0.02834	0.00060	231	13	180	4
3	151	300	0.50	0.05133	0.00251	0.22096	0.01037	0.03133	0.00044	203	9	199	3
4	760	1362	0.56	0.05121	0.00156	0.22219	0.00637	0.03138	0.00034	204	5	199	2
5	173	264	0.65	0.05352	0.00414	0.23200	0.01785	0.03168	0.00066	212	15	201	4
6	200	280	0.72	0.05142	0.00493	0.22666	0.02148	0.03179	0.00067	207	18	202	4
7	842	689	1.22	0.05055	0.00436	0.21878	0.01846	0.03128	0.00058	201	15	199	4
8	262	724	0.36	0.05124	0.00222	0.22398	0.00940	0.03158	0.00034	205	8	200	2
9	147	286	0.51	0.04926	0.00512	0.21618	0.02440	0.03116	0.00079	199	20	198	5
10	225	386	0.58	0.05200	0.00314	0.22550	0.01351	0.03142	0.00054	206	11	199	3
11	170	280	0.61	0.05278	0.00503	0.23068	0.02040	0.03212	0.00077	211	17	204	5
12	88	190	0.46	0.08482	0.00941	0.36275	0.03805	0.03189	0.00090	314	28	202	6
13	760	908	0.84	0.05377	0.00212	0.19798	0.00775	0.02656	0.00033	183	7	169	2
14	209	291	0.72	0.05755	0.00593	0.23585	0.02330	0.02985	0.00079	215	19	190	5
15	113	194	0.58	0.05132	0.00539	0.22070	0.02096	0.03146	0.00074	202	17	200	5
16	192	282	0.68	0.05616	0.00340	0.22098	0.01199	0.03124	0.00209	203	10	198	13
17	172	262	0.65	0.06732	0.00496	0.28658	0.02072	0.03104	0.00061	256	16	197	4
18	181	305	0.59	0.05354	0.00628	0.22935	0.02660	0.03118	0.00075	210	22	198	5
19	154	257	0.60	0.05438	0.00521	0.23386	0.02165	0.03130	0.00059	213	18	199	4
20	142	241	0.59	0.05007	0.00382	0.21880	0.01605	0.03175	0.00067	201	13	202	4

$\varepsilon_{Hf}(t)$ values of 2.5 to 3.9, with younger crustal model ages (T_{DM2}) of 889 to 964 Ma.

5.4. Re–Os dating

The Re–Os analytical results for three molybdenite samples from the Cuihongshan deposit are listed in Table 4. The total ^{187}Re and ^{187}Os concentrations vary from 486 to 663 ppb and 1.62 to 2.24 ppb, respectively. The model ages of the three samples range from 198.0 to 202.1 Ma, defining a weighted mean age of 200.1 ± 3.7 Ma, which is considered as the age of Mo mineralization.

6. Discussion

6.1. Age of magmatism and mineralization

As described in the deposit geology, two epochs of mineralizations are recognized in the Cuihongshan deposit. The early-epoch Fe mineralization was associated with the alkali–feldspar granite. The late-epoch Pb–Zn (Cu) and W–Mo mineralization was genetically linked to the syenogranite. Although a small portion of Fe orebodies were also formed during the late metallogenic epoch, they only account for a negligible percentage of the whole Fe reserves.

Zircon U–Pb dating suggests that the alkali–feldspar granite and the syenogranite have crystallization ages of 491.1 ± 2.4 Ma and 199.8 ± 1.8 Ma, respectively. The former could approximately represent the age of the predominant Fe mineralization, which should take place slightly after the crystallization of the alkali–feldspar granite. The later is consistent with the Re–Os model ages of the molybdenites (198.0–202.1 Ma), constraining the age of the Pb–Zn (Cu) and W–Mo mineralization to be 198.0 to 202.1 Ma.

6.2. Petrogenesis of the alkali–feldspar granite and the syenogranite

The alkali–feldspar granite and the syenogranite share common geochemical characteristics of high Fe/(Fe + Mg) ratio, high SiO_2 and $Na_2O + K_2O$ content, enrichment in Rb, Th, U and Pb, and depletion in Ba, Sr, Nb, Ta, P, Ti and Eu. These characteristics are typical of A-type granites (Collins et al., 1982; Eby, 1990, 1992; Sylvester, 1989; Whalen et al., 1987). In the discriminant diagrams of $Na_2O + K_2O$ versus Ga/Al (Fig. 9a) and $(Na_2O + K_2O)/CaO$ versus Zr + Nb + Ce + Y (Fig. 9b), all the samples fall into the A-type granite field, indicating that both the alkali–feldspar granite and the syenogranite are A-type granites.

Several mechanisms have been proposed to explain the generation of A-type granite magmas, involving partial melting of deep continental

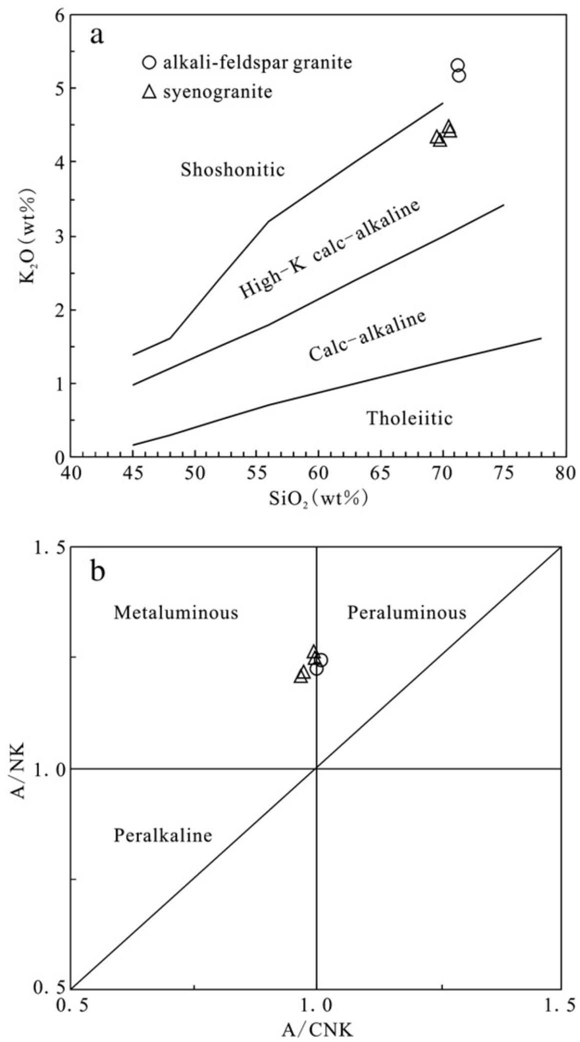

Fig. 6. Representative cathodoluminescence (CL) images of zircons from the alkali–feldspar granite (CHS-011) and the syenogranite (CHS-021). Small black circles indicate the positions for U–Pb dating, while large white circles indicate the Hf isotope analysis positions. The numbers marked in the center of the zircon grains represent the analyzed zircon numbers for U–Pb dating.

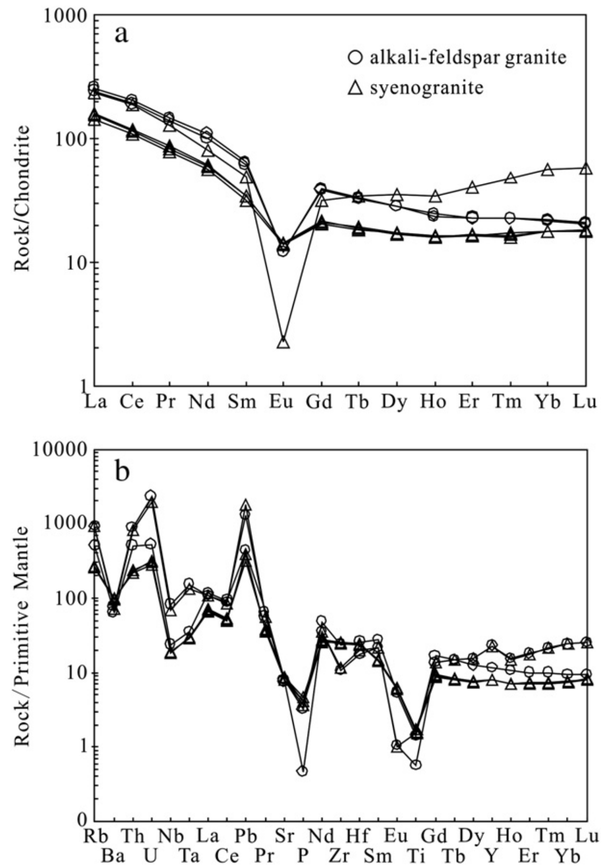

Fig. 7. Zircon U–Pb concordia diagrams and the weighted mean ^{206}Pb–^{238}U ages for the alkali–feldspar granite (CHS-011) and the syenogranite (CHS-021).

crust materials that were previously depleted by extraction of a hydrous felsic melt (Clemens et al., 1986; Collins et al., 1982; Creaser et al., 1991; Whalen et al., 1987), melting of hybridized lithospheric mantle (Whalen et al., 1996), and fractional crystallization from mantle-derived magmas with or without crustal contamination (Anderson et al., 2003; Jarrar et al., 2008; Pirajno et al., 2008; Smith et al., 1999; Turner et al., 1992).

The alkali–feldspar granite displays $\varepsilon_{Hf}(t)$ values of −3.7 to −1.3, with zircon Hf model ages (T_{DM2}) of 1414 to 1539 Ma, suggesting that the parental magma of the alkali–feldspar granite was probably formed by partial melting of an underlying Mesoproterozoic crust. Whereas the syenogranite yields positive $\varepsilon_{Hf}(t)$ values (2.5–3.9) and younger T_{DM2} ages (889–964 Ma), implying a depleted mantle source for the primary magmas. In addition, the depletions of Eu, Sr, Ba, P and Ti suggest that fractional crystallization occurred during the formation of the alkali–feldspar granite and the syenogranite. The negative Eu anomaly could be attributed to the fractionation of plagioclase and/or K-feldspar. The Sr depletion is indicative of the fractionation of plagioclase, while the Ba depletion may result from the fractionation of K-feldspar. The P and Ti depletions commonly indicate fractionation of apatite and Fe–Ti oxides during magma evolution.

Therefore, we suggest that the parental magma of the alkali–feldspar granite was originally derived from partial melting of the Mesoproterozoic crust and experienced subsequent fractional crystallization. Whereas the parental magma of the syenogranite predominantly originated from juvenile crustal materials which are related to a depleted mantle reservoir, and suffered fractional crystallization during the magma evolution.

6.3. Tectonic implications

Despite the controversies over the magma source of the A-type granites, they are generally considered to be associated with extensional tectonic environments (Eby, 1992; Stein and Hannah, 1985; Turner et al., 1992; Whalen et al., 1987). The A-type granites were subdivided into A_1 and A_2 groups by Eby (1992). The A_1 group represents the anorogenic granites which are mantle-derived but emplaced in intraplate settings such as continental rifts or other intraplate environments; the A_2 group represents the granites which are derived from melting of continental crust or underplated mafic crust and emplaced in various tectonic settings, especially post-collisional or post-orogenic settings. According to the Nb–Y–Ce (Fig. 10a) and Rb/Nb versus Y/Nb (Fig. 10b) geochemical discriminant diagrams, both the alkali–feldspar granite and the syenogranite fall into the A_2 group, suggesting their affinities to post-collisional or post-orogenic tectonic settings.

A number of A-type granites have been discovered in NE China (Shi et al., 2010; Wei et al., 2001; Wu et al., 2002; Yang et al., 2006; Zhou et al., 2012). They are formed during three major episodes: the Permian, late Triassic to early Jurassic, and early Cretaceous (Shao et al., 2012; Sun et al., 2005; Wu et al., 2002, 2011; Zheng et al., 2012). However, zircon U–Pb dating in this study indicate that the alkali–feldspar granite in the Cuihongshan mining district was formed at 491 Ma, which suggests a new episode for the formation of A-type granites in this area. Since

Table 3
Hf isotopic compositions of zircons from the alkali–feldspar granite and the syenogranite.

Spot	Age (Ma)	$^{176}Yb/^{177}Hf$	$^{176}Lu/^{177}Hf$	$^{176}Hf/^{177}Hf$	2σ	$(^{176}Hf/^{177}Hf)_i$	$\varepsilon_{Hf}(0)$	$\varepsilon_{Hf}(t)$	T_{DM1} (Ma)	T_{DM2} (Ma)	$f_{Lu/Hf}$
CHS-011 (alkali–feldspar granite)											
B1	487	0.000617	0.024122	0.282370	0.000035	0.282399	−14.2	−3.7	1233	1539	−0.98
B2	491	0.000740	0.029417	0.282412	0.000033	0.282415	−12.7	−2.2	1178	1456	−0.98
B3	489	0.000648	0.025613	0.282391	0.000037	0.282403	−13.5	−2.9	1205	1498	−0.98
B4	488	0.001000	0.040458	0.282409	0.000037	0.282429	−12.8	−2.4	1191	1469	−0.97
B5	496	0.000800	0.030312	0.282434	0.000039	0.282439	−12.0	−1.3	1150	1414	−0.98
CHS-021 (syenogranite)											
B1	199	0.001682	0.062658	0.282765	0.000022	0.282759	−0.2	3.9	703	889	−0.95
B2	202	0.002213	0.084179	0.282741	0.000021	0.282758	−1.1	3.1	748	939	−0.93
B3	198	0.001404	0.050549	0.282726	0.000018	0.282737	−1.6	2.5	753	964	−0.96
B4	200	0.001618	0.059516	0.282750	0.000020	0.282768	−0.8	3.4	723	917	−0.95
B5	202	0.001591	0.058320	0.282731	0.000019	0.282754	−1.4	2.8	749	954	−0.95

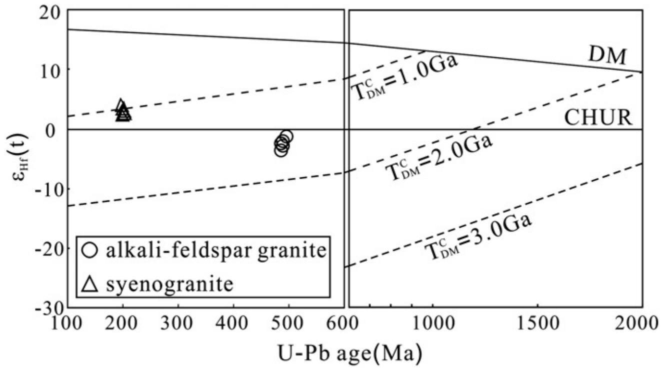

Fig. 8. $\varepsilon_{Hf}(t)$ values vs. U–Pb ages of zircons from the alkali–feldspar granite and the syenogranite.

the Cuihongshan deposit is located in the north segment of the Lesser Xing'an range, adjacent to the suture zone of the Songnen Block and the Xing'an Block, the formation of the alkali–feldspar granite may indicate that the tectonic setting has turned into extensional at about 491 Ma. Therefore, the final suturing between the Xing'an and Songnen Blocks may have taken place at nearly the same time as the suturing of the Xing'an and Erguna Blocks (494–480 Ma) (Ge et al., 2005, 2007), rather than the late Paleozoic as previously assumed (Sun et al., 2000; Zhao et al., 2010).

The syenogranite in the Cuihongshan deposit yields a crystallization age of 199.8 ± 1.8 Ma, which is consistent with numerous A-type granites distributed in NE China. The generation of these A-type granites, together with the occurrences of coeval metamorphic core complexes and mafic–ultramafic intrusions (Graham et al., 2001; Meng, 2003; Wu et al., 2002; Ying et al., 2010), suggest that NE China has turned into an extensional setting during the early Jurassic. The extensional setting could be attributed to three possible tectonic regimes: (1) post-collisional extension after the collision of the Mongol–Okhotsk Ocean; (2) back-arc extension related to the subduction of the Paleo-Pacific Ocean; (3) post-orogenic lithospheric extension after the final collision of the major crustal blocks in CAOB. The newly obtained paleomagnetic data suggest that the final closure of the Mongol–Okhotsk Ocean took place during the Early Cretaceous (Cogné et al., 2005; Metelkin et al., 2010; Pei et al., 2011), thereby giving little chance for inducing post-collisional extension in this region during the early Jurassic. In comparison, the subduction of the Paleo-Pacific Ocean started at the middle Jurassic (Chen et al., 2012), and the initial subduction occurred obliquely in a north or NNE direction (Kimura et al., 1990; Maruyama and Send, 1986), also unlikely to trigger back-arc extension during the early Jurassic. Therefore, we prefer that the early Jurassic extension is post-orogenic with respect to CAOB. Previous studies have confirmed that the eastern part of CAOB in NE China ended its compressive orogenic history in the late Triassic (Wu et al., 2002), lithospheric delamination is followed by decompressional melting of asthenospheric mantle (Shao et al., 2011). The lithospheric mantle would be partly replaced by the asthenosphere during this process, resulting in the transition from an enriched mantle to a depleted mantle (Daley and Depaolo, 1992; Perry et al., 1988; Wu et al., 2003). This is in accordance with our geochemical and Hf isotopic data, which suggest a depleted mantle source for the parental magma of the syenogranite.

7. Conclusion

The Cuihongshan Fe-polymetallic deposit is characterized by two-epoch mineralizations. The early-epoch Fe mineralization was genetically related to the alkali–feldspar granite and took place at about 491.1 ± 2.4 Ma, whereas the late-epoch Pb–Zn (Cu) and W–Mo mineralization was associated with the syenogranite, and occurred at about 198.0 to 202.1 Ma.

Both the alkali–feldspar granite and the syenogranite are A-type granites. The alkali–feldspar granite originated predominantly from partial melting of the Mesoproterozoic crustal materials, constraining the age of the final suturing between the Xing'an and Songnen Blocks earlier than 491 Ma. While the syenogranite was mainly generated by crystal fractionation from depleted-mantle-derived magmas, corresponding to the lithospheric delamination after the compressive orogenic history of the eastern CAOB.

Table 4
Re–Os data for molybdenites from the Cuihongshan deposit.

Sample no.	Ore type	Weight (g)	Re (ppm)		Os (ppb)		^{187}Re (ppm)		^{187}Os (ppb)		Model ages (Ma)	
			Measured	2σ	Measured	2σ	Measured	2σ	Measured	2σ	Measured	2σ
CHS-10	Veinlet-disseminated molybdenite	0.10052	0.7893	0.007	0.001	0.0046	0.4961	0.0044	1.639	0.016	198	3.1
CHS-12	Veinlet-disseminated molybdenite	0.10063	1.055	0.009	0.0008	0.0027	0.6632	0.0055	2.236	0.023	202.1	3.1
CHS-13	Quartz–molybdenite veinlet	0.10038	0.7732	0.0071	0.4334	0.5089	0.4859	0.0045	1.623	0.023	200.1	3.7

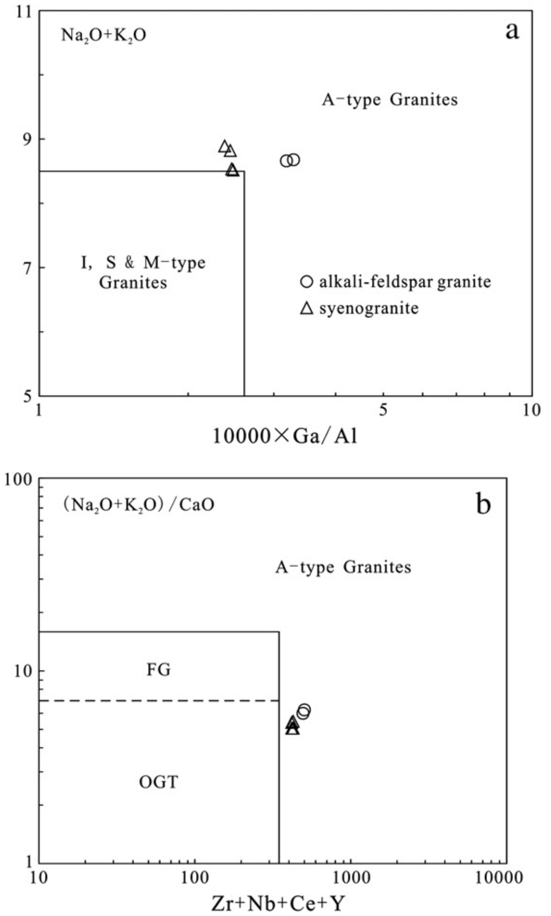

Fig. 9. (a) $Na_2O + K_2O$ vs. 10,000 × Ga/Al and (b) $Na_2O + K_2O/CaO$ vs. Zr + Nb + Ce + Y discriminant diagrams (after Whalen et al., 1987), showing the A-type nature of the alkali–feldspar granite and the syenogranite.

Acknowledgments

This research was funded by the Special Scientific Research Fund of Public Welfare Profession of China (Grant Nos. 201211008). The study benefited from discussion with Dr. D.H. Pi and Dr. S.F. Xiong. We deeply appreciate the detailed and constructive comments provided by Dr. H. Stein and another anonymous reviewer. Y.B. Cui, G.P. Zeng and C. Li are thanked for their assistance in LA ICP-MS U–Pb dating.

References

Anderson, I.C., Frost, C.D., Frost, B.R., 2003. Petrogenesis of the Red Mountain pluton, Laramie anorthosite complex, Wyoming: implications for the origin of A-type granite. Precambrian Res. 124, 243–267.

Blichert-Toft, J., Chauvel, C., Albarede, F., 1997. Separation of Hf and Lu for high-precision isotope analysis of rock samples by magnetic sector multiple collector ICP-MS. Contrib. Mineral. Petrol. 127, 248–260.

Chen, Y.J., Zhang, C., Li, N., Yang, Y.F., Deng, K., 2012. Geology of the Mo deposits in northeast China. J. Jilin Univ. (Earth Sci. Ed.) 42, 1223–1268 (in Chinese with English abstract).

Clemens, J.D., Holloway, J.R., White, A.J.R., 1986. Origin of an A-type granite — experimental constraints. Am. Mineral. 71, 317–324.

Cogné, J.P., Kravchinsky, V.A., Halim, N., Hankard, F., 2005. Late Jurassic–Early Cretaceous closure of the Mongol–Okhotsk Ocean demonstrated by new Mesozoic palaeomagnetic results from the Trans-Baikal area (SE Siberia). Geophys. J. Int. 163, 813–832.

Collins, W.J., Beams, S.D., White, A.J.R., Chappell, B.W., 1982. Nature and origin of A-type granites with particular reference to Southeastern Australia. Contrib. Mineral. Petrol. 80, 189–200.

Creaser, R.A., Price, R.C., Wormald, R.J., 1991. A-type granites revisited — assessment of a residual-source model. Geology 19, 163–166.

Daley, E.E., Depaolo, D.J., 1992. Isotopic evidence for lithospheric thinning during extension — southeastern Great-Basin. Geology 20, 104–108.

Du, A.D., He, H.L., Yin, N.W., Zou, X.Q., Sun, Y.L., Sun, D.Z., Cheng, S.Z., Qu, W.J., 1995. A study of the rhenium–osmium geochronometry of molybdenites. Acta Geol. Sin. Engl. Ed. 8, 171–181.

Du, A.D., Wu, S.Q., Sun, D.Z., Wang, S.X., Qu, W.J., Markey, R., Stein, H., Morgan, J., Malinovskiy, D., 2004. Preparation and certification of Re–Os dating reference materials: molybdenites HLP and JDC. Geostand. Geoanalytical Res. 28 (1), 41–52.

Du, M.Y., Li, C., Yang, N.F., Sun, Z.J., Wang, C.G., Yu, H.N., 2011. Metallogenic fluid inclusions and sulfur isotope characteristics of Cuihongshan iron polymetallic deposit. World Geol. 30, 538–543 (in Chinese with English abstract).

Eby, G.N., 1990. The A-type granitoids — a review of their occurrence and chemical characteristics and speculations on their petrogenesis. Lithos 26, 115–134.

Eby, G.N., 1992. Chemical subdivision of the A-type granitoids — petrogenetic and tectonic implications. Geology 20, 641–644.

Ge, W.C., Wu, F.Y., Zhou, C.Y., Rahman, A.A.A., 2005. Age of the granites in Tahe, north of the Great Xing'an range: constrains on the tectonic attribution of the Erguna Block. Chin. Sci. Bull. 50, 1239–1247.

Ge, W.C., Wu, F.Y., Zhou, C.Y., Zhang, J.H., 2007. Mineralization ages and geodynamic implications of porphyry Cu–Mo deposits in the east of Xingmeng orogenic belt. Chin. Sci. Bull. 52, 2407–2417.

Graham, S.A., Hendrix, M.S., Johnson, C.L., Badamgarav, D., Badarch, G., Amory, J., Porter, M., Barsbold, R., Webb, L.E., Hacker, B.R., 2001. Sedimentary record and tectonic implications of Mesozoic rifting in southeast Mongolia. Geol. Soc. Am. Bull. 113, 1560–1579.

Han, Z.X., Hao, Z.P., Hou, M., 1995. Metallogenic series of ore deposits related to Caledonian granitoids in XiaoHingganling region. Mineral Deposits 14, 293–302 (in Chinese with English abstract).

He, C., Li, S.Y., Gao, H., Wang, H.B., 2010. Geological condition of mineralization in the Cuihongshan skarn type Fe-polymetallic deposit. Heilongjiang Province. Jilin Geol. 29, 56–58 (in Chinese).

Hu, Z.C., Liu, Y.S., Gao, S., Liu, W.G., Zhang, W., Tong, X.R., Lin, L., Zong, K.Q., Li, M., Chen, H. H., Zhou, L., Yang, L., 2012. Improved in situ Hf isotope ratio analysis of zircon using newly designed X skimmer cone and jet sample cone in combination with the addition of nitrogen by laser ablation multiple collector ICP-MS. J. Anal. At. Spectrom. 27, 1391–1399.

Jarrar, G.H., Manton, W.I., Stern, R.J., Zachmann, D., 2008. Late Neoproterozoic A-type granites in the northernmost Arabian–Nubian Shield formed by fractionation of basaltic melts. Chem. Erde Geochem. 68, 295–312.

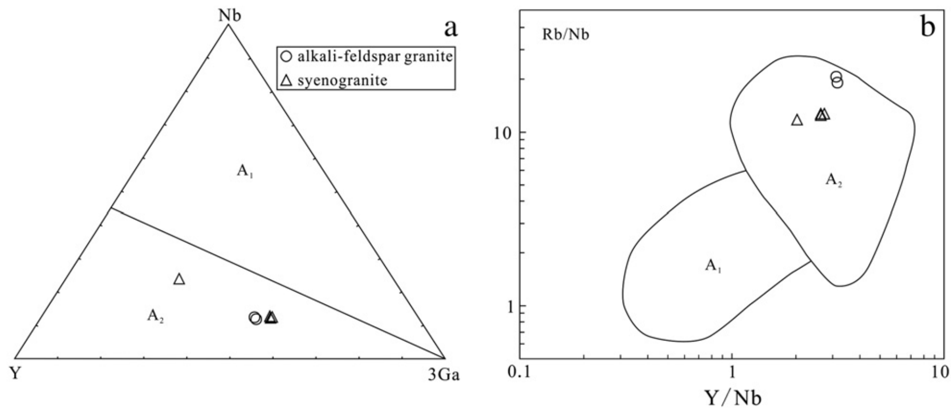

Fig. 10. (a) Nb–Y–Ce and (b) Rb/Nb vs. Y/Nb classification diagrams for A-type granites (Eby, 1992) showing the alkali–feldspar granite and the syenogranite belong to the A_2 group.

Kimura, G., Takahashi, M., Kono, M., 1990. Mesozoic collision extrusion tectonics in eastern Asia. Tectonophysics 181, 15–23.
Li, J.Y., 2006. Permian geodynamic setting of northeast China and adjacent regions: closure of the Paleo-Asian Ocean and subduction of the Paleo-Pacific Plate. J. Asian Earth Sci. 26, 207–224.
Li, X.R., Yang, H.Z., Shao, J., 2011. Characteristics of the magmatic rocks and mineralization age in the Cuihongshan Pb–Zn polymetallic deposit, Heilongjiang Province. Geol. Surv. Res. 35, 114–118 (in Chinese with English abstract).
Liu, Y.S., Hu, Z.C., Gao, S., Günther, D., Xu, J., Gao, C.G., Chen, H.H., 2008a. In situ analysis of major and trace elements of anhydrous minerals by LA–ICP-MS without applying an internal standard. Chem. Geol. 257, 34–43.
Liu, Y.S., Zong, K.Q., Kelemen, P.B., Gao, S., 2008b. Geochemistry and magmatic history of eclogues and ultramafic rocks from the Chinese continental scientific drill hole: subduction and ultrahigh-pressure metamorphism of lower crustal cumulates. Chem. Geol. 247, 133–153.
Liu, Y.S., Hu, Z.C., Zong, K.Q., Gao, C.G., Gao, S., Xu, J., Chen, H.H., 2010. Reappraisement and refinement of zircon U–Pb isotope and trace element analyses by LA–ICP-MS. Chin. Sci. Bull. 55, 1535–1546.
Ludwig, K.R., 2003. User's manual for Isoplot 3.00, a geochronological toolkit for Microsoft Excel. Berkeley Geochronological Center Spec. Publ. 4, 25–32.
Mao, J.W., Zhang, Z.C., Zhang, Z.H., Du, A.D., 1999. Re–Os isotopic dating of molybdenites in the Xiaoliugou W (Mo) deposit in the northern Qilian mountains and its geological significance. Geochim. Cosmochim. Acta 63, 1815–1818.
Mao, J.W., Zhang, Z.H., Yu, J.J., Wang, Y.T., Niu, B.G., 2003. Mesozoic large scale mineralization and geodynamic settings in North China and adjacent areas inspiration from the precise and accurate ages of metal deposits. Sci. China 33, 289–299.
Mao, J.W., Xie, G.Q., Zhang, Z.H., Li, X.F., Wang, Y.T., Zhang, C.Q., Li, Y.F., 2005. Mesozoic large-scale metallogenic pulses in North China and corresponding geodynamic settings. Acta Petrol. Sin. 21, 169–188 (in Chinese with English abstract).
Maruyama, S., Send, T., 1986. Orogeny and relative plate motions: example of the Japanese islands. Tectonophysics 127, 305–329.
Meng, Q.R., 2003. What drove late Mesozoic extension of the northern China–Mongolia tract? Tectonophysics 369, 155–174.
Metelkin, D.V., Vernikovsky, V.A., Kazansky, A.Y., Wingate, M.T.D., 2010. Late Mesozoic tectonics of Central Asia based on paleomagnetic evidence. Gondwana Res. 18, 400–419.
Pei, J.L., Sun, Z.M., Liu, J., Liu, J., Wang, X.S., Yang, Z.Y., Zhao, Y., Li, H.B., 2011. A paleomagnetic study from the Late Jurassic volcanics (155 Ma), North China: implications for the width of Mongol–Okhotsk Ocean. Tectonophysics 510, 370–380.
Perry, F.V., Baldridge, W.S., Depaolo, D.J., 1988. Chemical and isotopic evidence for lithospheric thinning beneath the Rio-Grande rift. Nature 332, 432–434.
Pirajno, F., Mao, J.W., Zhang, Z.C., Zhang, Z.H., Chai, F.M., 2008. The association of mafic–ultramafic intrusions and A-type magmatism in the Tian Shan and Altay orogens, NW China: implications for geodynamic evolution and potential for the discovery of new ore deposits. J. Asian Earth Sci. 32, 165–183.
Qi, J.P., Chen, Y.J., Franco, P., 2005. Geological characteristics and tectonic setting of the epithermal deposits in the northeast China. J. Mineral. Petrol. 25, 47–59 (in Chinese with English abstract).
Rickwood, P.C., 1989. Boundary lines within petrologic diagrams which use oxides of major and minor elements. Lithos 22, 247–263.
Segal, I., Halicz, L., Platzner, I.T., 2003. Accurate isotope ratio measurements of ytterbium by multiple collection inductively coupled plasma mass spectrometry applying erbium and hafnium in an improved double external normalization procedure. J. Anal. At. Spectrom. 18, 1217–1223.
Selby, D., Creaser, R.A., 2004. Macroscale NTIMS and microscale LA–MC–ICP-MS Re–Os isotopic analysis of molybdenite: testing spatial restrictions for reliable Re–Os age determinations, and implications for the decoupling of Re and Os within molybdenite. Geochim. Cosmochim. Acta 68, 3897–3908.
Shao, J., Li, X.R., Yang, H.Z., 2011. Zircon SHRIMP U–Pb dating of granite in the Cuihongshan polymetallic deposit and its geological implications. Acta Geosci. Sin. 32, 163–170 (in Chinese with English abstract).
Shao, J., Yang, H.Z., Jia, B., Peng, M.S., 2012. Geological characteristics and ore-forming age of Luming Mo deposit in Heilongjiang Province. Mineral Deposits 31, 1301–1310 (in Chinese with English abstract).
Shi, Y.R., Liu, D.Y., Miao, L.C., Zhang, F.Q., Jian, P., Zhang, W., Hou, K.J., Xu, J.Y., 2010. Devonian A-type granitic magmatism on the northern margin of the North China Craton: SHRIMP U–Pb zircon dating and Hf-isotopes of the Hongshan granite at Chifeng, Inner Mongolia, China. Gondwana Res. 17, 632–641.
Smith, D.R., Noblett, J., Wobus, R.A., Unruh, D., Douglass, J., Beane, R., Davis, C., Goldman, S., Kay, G., Gustavson, B., Saltoun, B., Stewart, J., 1999. Petrology and geochemistry of late-stage intrusions of the A-type, mid-Proterozoic Pikes Peak batholith (Central Colorado, USA): implications for petrogenetic models. Precambrian Res. 98, 271–305.
Smoliar, M.I., Walker, R.J., Morgan, J.W., 1996. Re–Os ages of group IIA, IIIA, IVA, and IVB iron meteorites. Science 271, 1099–1102.
Stein, H.J., Hannah, J.L., 1985. Movement and origin of ore fluids in Climax-type systems. Geology 13, 469–474.
Stein, H., Schersten, A., Hannah, J., Markey, R., 2003. Subgrain-scale decoupling of Re and Os-187 and assessment of laser ablation ICP-MS spot dating in molybdenite. Geochim. Cosmochim. Acta 67, 3673–3686.
Sun, S.S., McDonough, W.F., 1989. Chemical and isotopic systematics of oceanic basalts: implication for the mantle composition and process. In: Saunder, A.D., Norry, M.J. (Eds.), Magmatism in the Ocean Basins: Geological Society of London Special Publication, London. , Vol. 42, pp. 313–345.
Sun, D.Y., Wu, F.Y., Li, H.M., Lin, Q., 2000. Age of the post-orogenic A-type granites in the northwestern Lesser Xing'an range and their relationship with the east part of the Suolunshan–Hegenshan–Zhalaite suture zone. Chin. Sci. Bull. 45, 2217–2222.
Sun, D.Y., Wu, F.Y., Li, H.M., Lin, Q., 2001. Emplacement age of the postorogenic A-type granites in Northwestern Lesser Xing'an Ranges, and its relationship to the eastward extension of Suolushan–Hegenshan–Zhalaite collisional suture zone. Chin. Sci. Bull. 46, 427–432.
Sun, D.Y., Wu, F.Y., Gao, S., Lu, X.P., 2005. Confirmation of two episodes of A-type granite emplacement during Late Triassic and Early Jurassic in the central Jilin Province, and their constraints on the structural pattern of Eastern Jilin–Heilongjiang Area, China. Earth Sci. Frontiers 12, 263–275 (in Chinese with English abstract).
Sun, J.G., Han, S.J., Zhang, Y., Xing, S.W., Bai, L.A., 2013. Diagenesis and metallogenetic mechanisms of the Tuanjiegou gold deposit from the Lesser Xing'an Range, NE China: zircon U–Pb geochronology and Lu–Hf isotopic constraints. J. Asian Earth Sci. 62, 373–388.
Sylvester, P.J., 1989. Post-collisional alkaline granites. J. Geol. 97, 261–280.
Turner, S.P., Foden, J.D., Morrison, R.S., 1992. Derivation of some A-type magmas by fractionation of basaltic magma — an example from the Padthaway Ridge, South Australia. Lithos 28, 151–179.
Wang, H.Z., Mo, X.X., 1995. An outline of the tectonic evolution of China. Episodes 18, 6–16.
Wei, C.S., Zheng, Y.F., Zhao, S.F., Valley, J.W., 2001. Oxygen isotope evidence for two-stage water–rock interactions of the Nianzishan A-type granite in NE China. Chin. Sci. Bull. 46, 727–731.
Whalen, J.B., Currie, K.L., Chappell, B.W., 1987. A-type granites — geochemical characteristics, discrimination and petrogenesis. Contrib. Mineral. Petrol. 95, 407–419.
Whalen, J.B., Jenner, G.A., Longstaffe, F.J., Robert, F., Gariepy, C., 1996. Geochemical and isotopic (O Nd, Pb and Sr) constraints on a type granite petrogenesis based on the topsails igneous suite, Newfoundland Appalachians. J. Petrol. 37, 1463–1489.
Wu, F.Y., Jahn, B.M., Wilde, S., Sun, D.Y., 2000. Phanerozoic crustal growth: U–Pb and Sr–Nd isotopic evidence from the granites in northeastern China. Tectonophysics 328, 89–113.
Wu, F.Y., Sun, D.Y., Li, H.M., Jahn, B.M., Wilde, S., 2002. A-type granites in northeastern China: age and geochemical constraints on their petrogenesis. Chem. Geol. 187, 143–173.
Wu, F.Y., Ge, W.C., Sun, D.Y., Guo, C.L., 2003. Discussions on the lithospheric thinning in eastern china. Earth Sci. Frontiers 10, 51–60 (in Chinese with English abstract).
Wu, F.Y., Yang, J.H., Wilde, S.A., Zhang, X.O., 2005. Geochronology, petrogenesis and tectonic implications of Jurassic granites in the Liaodong Peninsula, NE China. Chem. Geol. 221, 127–156.
Wu, F.Y., Yang, J.H., Lo, C.H., Wilde, S.A., Sun, D.Y., Jahn, B.M., 2007. The Heilongjiang Group: A Jurassic accretionary complex in the Jiamusi Massif at the western Pacific margin of northeastern China. Island Arc 16, 156–172.
Wu, F.Y., Sun, D.Y., Ge, W.C., Zhang, Y.B., Grant, M.L., Wilde, S.A., Jahn, B.M., 2011. Geochronology of the Phanerozoic granitoids in northeastern China. J. Asian Earth Sci. 41, 1–30.
Xu, W.L., Sun, D.Y., Zhou, Y., 1994. Manzhouli–Suifenhe Geoscience Transect Magmatism and Crust Structure. Geological Publishing House, Beijing pp. 85–94 (in Chinese).
Yang, J.H., Wu, F.Y., Chung, S.L., Wilde, S.A., Chu, M.F., 2006. A hybrid origin for the Qianshan A-type granite, northeast China: geochemical and Sr–Nd–Hf isotopic evidence. Lithos 89, 89–106.
Yang, Y.C., Han, S.J., Sun, D.Y., Guo, J., Zhang, S.J., 2012. Geological and geochemical features and geochronology of porphyry molybdenum deposits in the Lesser Xing'an Range–Zhangguangcai Range metallogenic belt. Acta Petrol. Sin. 28, 379–390 (in Chinese with English abstract).
Yin, B.C., Ran, Q.C., 1997. Metallogenic evolution in Xiaohingganling–Zhangguangcailing region, Heilongjiang Province. Mineral Deposits 16, 235 (in Chinese with English abstract).
Ying, J.F., Zhou, X.H., Zhang, L.C., Wang, F., Zhang, Y.T., 2010. Geochronological and geochemical investigation of the late Mesozoic volcanic rocks from the Northern Great Xing'an Range and their tectonic implications. Int. J. Earth Sci. 99, 357–378.
Zhang, J.H., Gao, S., Ge, W.C., Wu, F.Y., Yang, J.H., Wilde, S.A., Li, M., 2010a. Geochronology of the Mesozoic volcanic rocks in the Great Xing'an Range, northeastern China: implications for subduction-induced delamination. Chem. Geol. 276, 144–165.
Zhang, Z.C., Mao, J.W., Wang, Y.B., Pirajno, F., Liu, J.L., Zhao, Z.D., 2010b. Geochemistry and geochronology of the volcanic rocks associated with the Dong'an adularia — sericite epithermal gold deposit, Lesser Hinggan Range, Heilongjiang province, NE China: constraints on the metallogenesis. Ore Geol. Rev. 37, 158–174.
Zhao, H.D., Liu, Y., Deng, J.F., Xiao, Q.H., Ling, M.A.L., Yang, Y.J., 2009. Characteristics and significances of rapakivi in Yichun area of Xiaoxinganling, Heilongjiang Province. Geol. China 36, 658–668 (in Chinese with English abstract).
Zhao, Z., Chi, X.G., Pan, S.Y., Liu, J.F., Sun, W., Hu, Z.C., 2010. Zircon U — Pb LA — ICP-MS dating of Carboniferous volcanics and its geological significance in the northwestern Lesser Xing'an Range. Acta Petrol. Sin. 26, 2452–2464 (in Chinese with English abstract).
Zheng, Q.B., Wang, Y., Zhang, G.Y., Jin, Z.Y., 2012. Confirmation of Late Triassic A-type granite and their geochemical constraints on structural setting in eastern Heilongjiang. World Geol. 31, 471–478 (in Chinese with English abstract).
Zhou, J.B., Wilde, S.A., Zhao, G.C., Zhang, X.Z., Zheng, C.Q., Wang, H., 2010. New SHRIMP U — Pb zircon ages from the Heilongjiang high-pressure belt: constraints on the Mesozoic evolution of NE china. Am. J. Sci. 310, 1024–1053.
Zhou, Z.H., Mao, J.W., Lyckberg, P., 2012. Geochronology and isotopic geochemistry of the A-type granites from the Huanggang Sn — Fe deposit, southern Great Hinggan Range, NE China: implication for their origin and tectonic setting. J. Asian Earth Sci. 49, 272–286.